4. E. J. Ginsburg, C. B. Gorman, S. R. Marder, R. H. Grubbs, *J. Am. Chem. Soc.* **111**, 7621 (1989).
5. C. B. Gorman, E. J. Ginsburg, S. R. Marder, R. H. Grubbs, *Angew. Chem. Adv. Mater.* **101**, 1603 (1989).
6. C. Schaverien, J. Dewan, R. R. Schrock, *J. Am. Chem. Soc.* **108**, 2771 (1986).
7. A. M. Saxman, R. Liepins, M. Aldissi, *Prog. Polym. Sci.* **11**, 57 (1985).
8. M. Aldissi, *Inherently Conducting Polymers: Processing, Fabrication, Applications, Limitations* (Noyes Data, Park Ridge, NJ, 1989).
9. H. Shirakawa, E. J. Louis, A. G. MacDiarmid, C. K. Chiang, A. J. Heeger, *J. Chem. Soc. Chem. Commun.* **1977**, 578 (1977).
10. R. Z. Bachrach, in *Metal-Semiconductor Schottky Barrier Junctions and Their Applications*, B. L. Sharma, Ed. (Plenum, New York, 1984), pp. 93–99; S. M. Sze, *Physics of Semiconductor Devices* (Wiley, New York, 1981), pp. 245–311.
11. N. S. Lewis, *J. Electrochem. Soc.* **131**, 2496 (1984).
12. A. L. Fahrenbruch and R. H. Bube, *Fundamentals of Solar Cells* (Academic Press, New York, 1983), chap. 6.
13. ———, *ibid.*, chap. 7.
14. D. B. Neal *et al.*, *Synth. Met.* **28**, D711 (1989); M. C. J. Young, R. H. Tredgold, P. Hodge, *R. Soc. Chem. Spec. Publ.* **69**, 354 (1989); R. H. Tredgold, M. C. J. Young, P. Hodge, E. Khoshdel, *Thin Solid Films* **151**, 441 (1987).
15. F. L. Klavetter and R. H. Grubbs, *Synth. Met.* **28**, D105 (1989).
16. S. H. Askari, S. D. Rughooputh, F. Wudl, A. J. Heeger, *Polym. Prep.* **30**, 157 (1989); S. Hotta, S. D. D. V. Rughooputh, A. J. Heeger, F. Wudl, *Macromolecules* **20**, 212 (1987); K. Y. Jen, R. L. Oboodi, R. L. Elsenbaumer, *Polym. Mater. Sci. Eng.* **53**, 79 (1985); K. Y. Jen, M. Maxfield, L. W. Shacklette, R. L. Elsenbaumer, *J. Chem. Soc. Chem. Commun.* **4**, 309 (1987); S. D. D. V. Rughooputh, M. Nowak, S. Hotta, A. J. Heeger, F. Wudl, *Synth. Met.* **21**, 41 (1987); D. C. Bott *et al.*, *ibid.* **14**, 245 (1986); J. Edwards, W. J. Feast, D. Bott, *Polymer* **25**, 395 (1984).
17. A. J. Frank, S. Glenis, A. J. Nelson, *J. Phys. Chem.* **93**, 3818 (1989); M. Ozaki, D. Peebles, B. R. Weinberger, A. J. Heeger, A. G. MacDiarmid, *J. Appl. Phys.* **51**, 4252 (1980); M. J. Cohen and J. S. Harris, Jr., *Appl. Phys. Lett.* **33**, 812 (1978).
18. F. Garnier and G. Horowitz, *Synth. Met.* **18**, 693 (1987).
19. T. Skotheim, O. Inganas, J. Prejza, I. Lundstroem, *Mol. Cryst. Liq. Cryst.* **83**, 1361 (1982); T. Skotheim and I. Lundstroem, *J. Electrochem. Soc.* **129**, 894 (1982); T. A. Skotheim and O. Inganas, *ibid.* **132**, 2116 (1985); G. Nagasubramanian, S. DiStefano, J. Moacanin, in *Polymers for Advanced Technologies: IUPAC International Symposium*, M. Lewin, Ed. (VCH, New York, 1988), pp. 261–268.
20. Supported by NSF grant CHE8814694 and ONR grant N001488K0208. C.B.G. thanks the Jet Propulsion Laboratory, Caltech, for a research fellowship. E.J.G. thanks IBM for a graduate fellowship, and A.K. thanks the Department of Education for a graduate fellowship. Contribution 8134 from the Arnold and Mabel Beckman Laboratory of Chemical Synthesis and the Arthur Amos Noyes Laboratory of Chemical Physics.

7 May 1990; accepted 26 June 1990

Inclusion of Thermal Motion in Crystallographic Structures by Restrained Molecular Dynamics

PIET GROS, WILFRED F. VAN GUNSTEREN, WIM G. J. HOL

A protein crystal structure is usually described by one single structure, which largely omits the dynamical behavior of the molecule. A molecular dynamics method with a time-averaged crystallographic restraint was used to overcome this limitation. This method yields an ensemble of structures in which all possible thermal motions are allowed, that is, in addition to isotropic distributions, anisotropic and anharmonic positional distributions occur as well. In the case of bovine pancreatic phospholipase A_2, this description markedly improves agreement with the observed x-ray diffraction data compared to the results of the classical one-model structure description. Time-averaged crystallographically restrained molecular dynamics reveals large mobilities in the loops involved in lipid bilayer association.

THE CLASSICAL REPRESENTATION OF a protein crystal structure is basically limited to a single site isotropic model for each atom. Because of the limited number of x-ray diffraction data from large biomacromolecules, the thermal parameters of each atom, which describe the fluctuations around the average position, cannot be refined anisotropically. Furthermore, the atomic motions in large proteins may be more complicated and include anharmonicity, as shown in the segmented anisotropic refinement of bovine ribonuclease A (*1*). The inability to model anharmonicity and anisotropy gives rise to systematic errors present in the model (*2*). In molecular dynamics (MD) simulations, the configurational space is explored and thus anisotropic as well as anharmonic distributions of the atoms are obtained as represented by the trajectory of the atoms. However, calculating diffraction data from an unrestrained MD simulation (*3*) yielded, in the case of bovine pancreatic trypsin inhibitor, a low agreement with the experimental data, that is, a high crystallographic residual R ($= \Sigma||\mathbf{F}_o| - |\mathbf{F}_c||/\Sigma|\mathbf{F}_o|$, where $\mathbf{F}_o$ and $\mathbf{F}_c$ are the observed and calculated structure factors, respectively) of 0.52.

We have combined MD simulations with crystallographic data by restraining the structure factor amplitudes taken over the whole ensemble of structures to the observed x-ray data. In this crystallographically restrained MD simulation the following target function is used:

$$E = E_{\text{phys}} + \frac{1}{\sigma_x^2} \sum_{\mathbf{s}} (|\mathbf{F}_o(\mathbf{s})| - k|\langle \mathbf{F}_c(\mathbf{s}) \rangle|)^2 \quad (1)$$

where E_{phys} represents the bond, bond angle, dihedral, improper dihedral, electrostatic, and Lennard-Jones interaction potentials (*4*), $\mathbf{s}$ is the reciprocal lattice vector, k is a scale factor, and σ_x is a weighting factor. The essential difference with the MD crystallographic refinement procedure (*5, 6*) is the use of the ensemble average of calculated structure factors, $\langle \mathbf{F}_c \rangle$, instead of the structure factors of one single structure. We considered similar arguments as Torda *et al.* (*7, 8*) for combining nuclear magnetic resonance–nuclear Overhauser effect data and MD procedures and used a time-weighted, or "running," average for the calculation of $\langle \mathbf{F}_c \rangle$ in the restraint:

$$\langle \mathbf{F}_c(\mathbf{s}) \rangle_{t'} = \frac{1}{\tau_x(1 - e^{-t'/\tau_x})} \int_0^{t'} e^{-(t' - t)/\tau_x} \mathbf{F}_c^t(\mathbf{s}) dt \quad (2)$$

where τ_x is the structure factor–memory relaxation time and $\mathbf{F}_c^t(\mathbf{s})$ is a structure factor based on an individual structure at time point t from the trajectory and depends only on positional parameters. No individual thermal parameters are assigned to the atoms. The spread of the atoms as found in the crystal is now represented by the spatial distributions of the atoms in the generated ensemble.

Bovine phospholipase A_2 ($BPLA_2$) is a 123-residue enzyme that degrades phospholipids and acts primarily on aggregated lipids as in bilayers or in micelles (*9*). Its crystal structure has been determined at 1.7 Å resolution and refined to a crystallographic residual of 0.171 (*10*). On the basis of the classic representation of the molecule, with three positional parameters and one thermal parameter per atom, the structure-function relation of phospholipases A_2 has been studied in detail (*11–13*).

We calculated an ensemble of $BPLA_2$ structures that was restrained according to Eqs. 1 and 2 to the available x-ray diffraction data. It appeared that crystallographically restrained MD gave a significant better agreement between observed and calculated x-ray data (Fig. 1A) than either conventional x-ray refinement procedure (*10*) or unrestrained MD (*3*). The improvement obtained by modeling anisotropy and anharmonicity is most dramatic in the higher resolution shells (Fig. 1A). For instance, for

BIOSON Research Institute, Department of Chemistry, University of Groningen, Nijenborgh 16, 9747 AG Groningen, The Netherlands.

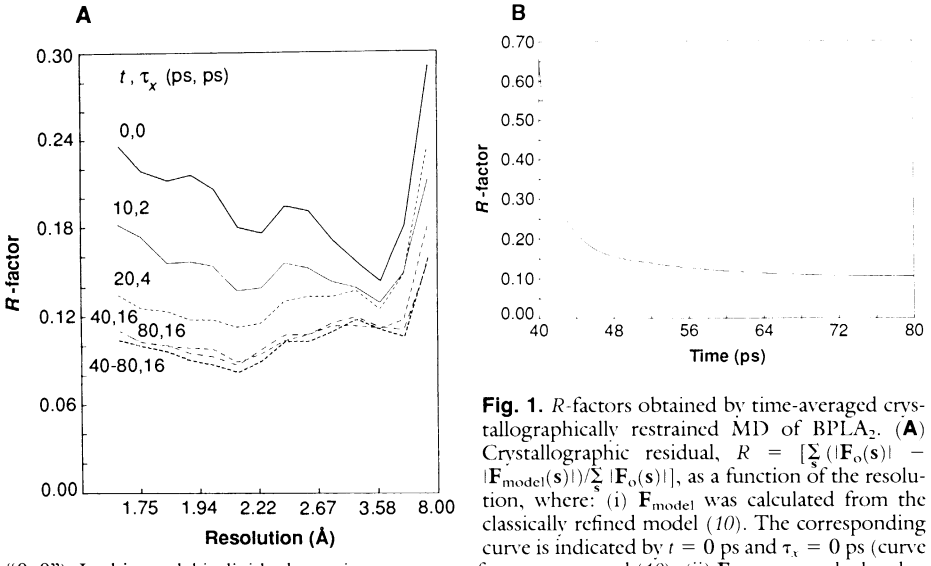

Fig. 1. R-factors obtained by time-averaged crystallographically restrained MD of $BPLA_2$. (**A**) Crystallographic residual, $R = [\sum_s (|\mathbf{F}_o(\mathbf{s})| - |\mathbf{F}_{model}(\mathbf{s})|)/\sum_s |\mathbf{F}_o(\mathbf{s})|]$, as a function of the resolution, where: (i) $\mathbf{F}_{model}$ was calculated from the classically refined model (*10*). The corresponding curve is indicated by $t = 0$ ps and $\tau_x = 0$ ps (curve "0, 0"). In this model individual atomic temperature factors were used (*10*); (ii) $\mathbf{F}_{model}$ was calculated as weighted averages with Eq. 2, from the MD run at times $t = 10$ ps with $\tau_x = 2$ ps (curve "10, 2"), $t = 20$ ps with $\tau_x = 4$ ps (curve "20, 4"), $t = 40$ ps with $\tau_x = 16$ ps (curve "40, 16"), and $t = 80$ ps also with $\tau_x = 16$ ps (curve "80, 16"). During the run a temperature factor of 1 Å^2 was assigned to each atom; and (iii) $\mathbf{F}_{model}$ was calculated as the average structure factors from the trajectory $t = 40$ to 80 ps with $\tau_x = 16$ ps (curve "40–80, 16"). Additional overall scaling of $|\mathbf{F}_{model}|$ to $|\mathbf{F}_o|$, yielding a scale factor of $k = 1.082$ and a relative overall temperature factor $B_{iso} = 1.028$ Å^2, reduced the residual from 0.104 to 0.098. (**B**) The R-factor, based on the averaged $\mathbf{F}_c$, as function of time from $t = 40$ ps to $t = 80$ ps. At $t = 40$ ps one single structure had a crystallographic residual of 0.65. After averaging over a time span of 40 ps, that is, 20,000 structures, the R-factor dropped to 0.104, without additional overall scaling (*14*).

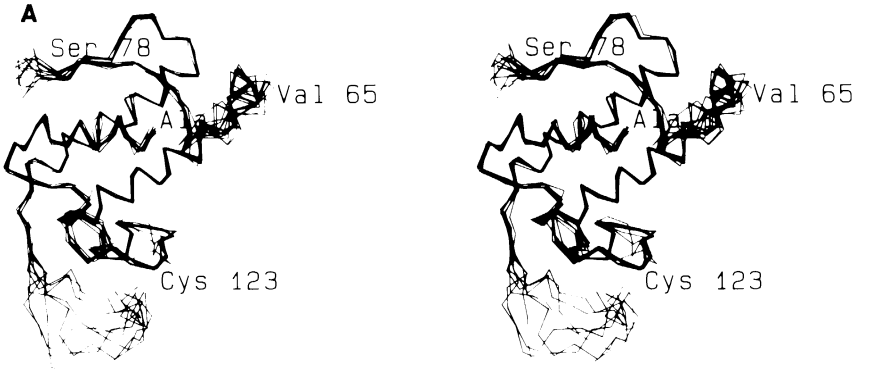

Fig. 2. Mobility of $BPLA_2$ as revealed by crystallographically restrained MD. (**A**) The Cα tracings of eight structures of $BPLA_2$ as observed at 4-ps intervals for $t = 40$ to 68 ps. From $t = 48$ to 60 ps some residues from the loop 112 to 123 occupied positions of a neighboring molecule, which shows that crystal contacts should be treated explicitly in these calculations either by van der Waals restraints (*22*) in a vacuo simulation or by simulating a whole unit cell with periodic boundary conditions. (**B**) Comparison between isotropic temperature factors averaged over the main chain atoms as determined in the classical refinement (*10*) (solid lines) and as retrieved from the trajectory collected from $t = 40$ to 80 ps (dashed lines). The isotropic B-factors from the MD ensemble were obtained as a mean square fluctuation around one single average conformation of the protein, which means that these B-factors for the hypermobile regions contain contributions related to different atomic equilibrium positions and therefore reflect merely their hypermobility. The correlation coefficient between the classical crystallographic temperature factors and the isotropic temperature factors derived from the simulation is 0.45 for all 957 non-hydrogen atoms; disregarding the outliers ($\Delta B > 20$ Å) improves the correlation to 0.73 for 640 atoms.

reflections between 1.75 and 1.70 Å resolution, the R-factor drops from 0.236 to 0.104. At low resolution the R-factor remains somewhat higher, (0.159 for reflections between 8.0 and 6.3 Å resolution) because for these data the solvent continuum contributes significantly to the structure amplitudes. In this explorative study the bulk water in the crystal was not simulated and this omission caused errors at low resolution. During the simulation all temperature factors were kept at 1 Å^2 and all atoms fluctuated around their average positions. Thus a high crystallographical residual, $R \sim 0.65$, was observed for each individual structure of the ensemble. After averaging the structure factors of all structures in the ensemble, the R-factor dropped to 0.098, when all data with $|\mathbf{F}_o| > \sigma_\mathbf{F}$ between 8 and 1.7 Å resolution were used (see Fig. 1B), whereas the residual of the classically refined model is 0.171 (*10*). This reduction in R-factor was obtained while a good geometry of the structures in the trajectory was retained (*14–17*).

Perhaps more important is that the ensemble of structures contains information on the mobility of the protein molecule in the crystal lattice. An impression of the atomic fluctuations is obtained by inspecting Cα tracings of $BPLA_2$ models occurring at 4-ps intervals (Fig. 2A). As expected, the interior of the molecules shows only small fluctuations around the average atomic positions. In contrast, some surface residues appear to be highly mobile, even with respect to their backbone conformation. This motion involves residues Gly^{30} to Gly^{35}, Val^{62} to Val^{66}, Ser^{77} to Glu^{81}, and the COOH-terminal loop Asn^{117} to Cys^{123} (Fig. 2B). These last three regions are also the only three regions that differ significantly between phospholipase A_2 from the *Crotalus atrox* venom and the bovine enzyme (*13*). Furthermore, loops 30 to 35, 62 to 66, and 117 to 123 are thought to be part of the binding site of aggregated phospholipids (*18*). Hence, the observed flexibility for these loops could well be important for the interaction of the protein with the layer of polar headgroups of the aggregated phospholipids.

In the case of $BPLA_2$ the mobile loops appear to have one major conformation, which is observed in the electron density map. As an example we show in Fig. 3 two residues from the mobile loop consisting of residues 77 to 81. The electron density of the single distinct conformation is reproduced with the structure factors of the ensemble in a $(2|\mathbf{F}_o| - |\langle\mathbf{F}_c\rangle|)\exp i\alpha_{av}$ map (Fig. 3B), where α_{av} stands for the phase of $\langle\mathbf{F}_c\rangle$. An electron density map, similar to the one shown in Fig. 3B, is obtained when

only calculated data are used, that is, with coefficients $(|\langle \mathbf{F}_c \rangle|)\exp i\alpha_{av}$. This result shows that the large spatial distribution of the atoms seen in Fig. 3C results in a clear electron density for this loop that is missing only the electron density of the side chain of Asn^{79}. The appearance of electron density at the position of the side chain atoms of Asn^{79} in the classical map (Fig. 3A) might be caused by model bias from the full occupancy of the single site isotropic model. Furthermore, the discrepancy in isotropic temperature factors (Fig. 2B) for these very mobile regions can be explained by the fact that classically determined *B*-factors refer to the main conformation only, whereas the *B*-factors retrieved from the ensemble take all major and minor conformations into account. This result means that the interpretation of the most frequently occurring distinct conformation for the loop 77 to 81 in the conventionally refined structure is essentially correct, although this conformation is only valid for a limited fraction of structures.

An important parameter in these crystallographically restrained MD simulations is τ_x. The crystallographic restraint (see Eq. 1) is nonconservative and leads to heating, which is dependent on the magnitude of τ_x. The longer τ_x is, the less heating is observed (*14*). According to (*8*), τ_x should be chosen to be as long as possible but still roughly an order of magnitude smaller than the length of the simulation.

The method we present can be extended by including the solvent continuum and the crystal lattice explicitly in the simulation, which implies application of the periodic boundary conditions (*19*) to the unit cell and addition of the bulk water. Most likely this should improve the correlation between observed and calculated x-ray data, particularly at low resolution. Additional improvement can then be obtained by replacing the vacuo parameter settings of the MD force field by the physically more realistic parameter set used for simulation in water (*4, 20*). Furthermore, to model static disorder of a crystal it may be required to perform separate MD runs with different starting models. Hence, when simulating a crystal explicitly and sampling for a longer time (τ_x), an even more reliable ensemble of structures and further agreement with the experimental data is to be expected.

In the case of $BPLA_2$ only a few minor coordinate errors were present in the starting model of the simulation, for instance, wrongly placed Cδ of Leu^{41} or the wrongly placed solvent-accessible side chain of Arg^{43}. These errors were corrected automatically in an early stage of the simulation, that is when τ_x was small and the individual isotropic temperature factors were still largely present. Thus it is conceivable that the technique might also be useful in the refinement of the single structure itself. Brünger (*21*) showed that when a series of structures is generated by classical MD refinement, large fluctuations may indicate either disordered or erroneously fitted segments of the molecule. For the time-averaged restrained simu-

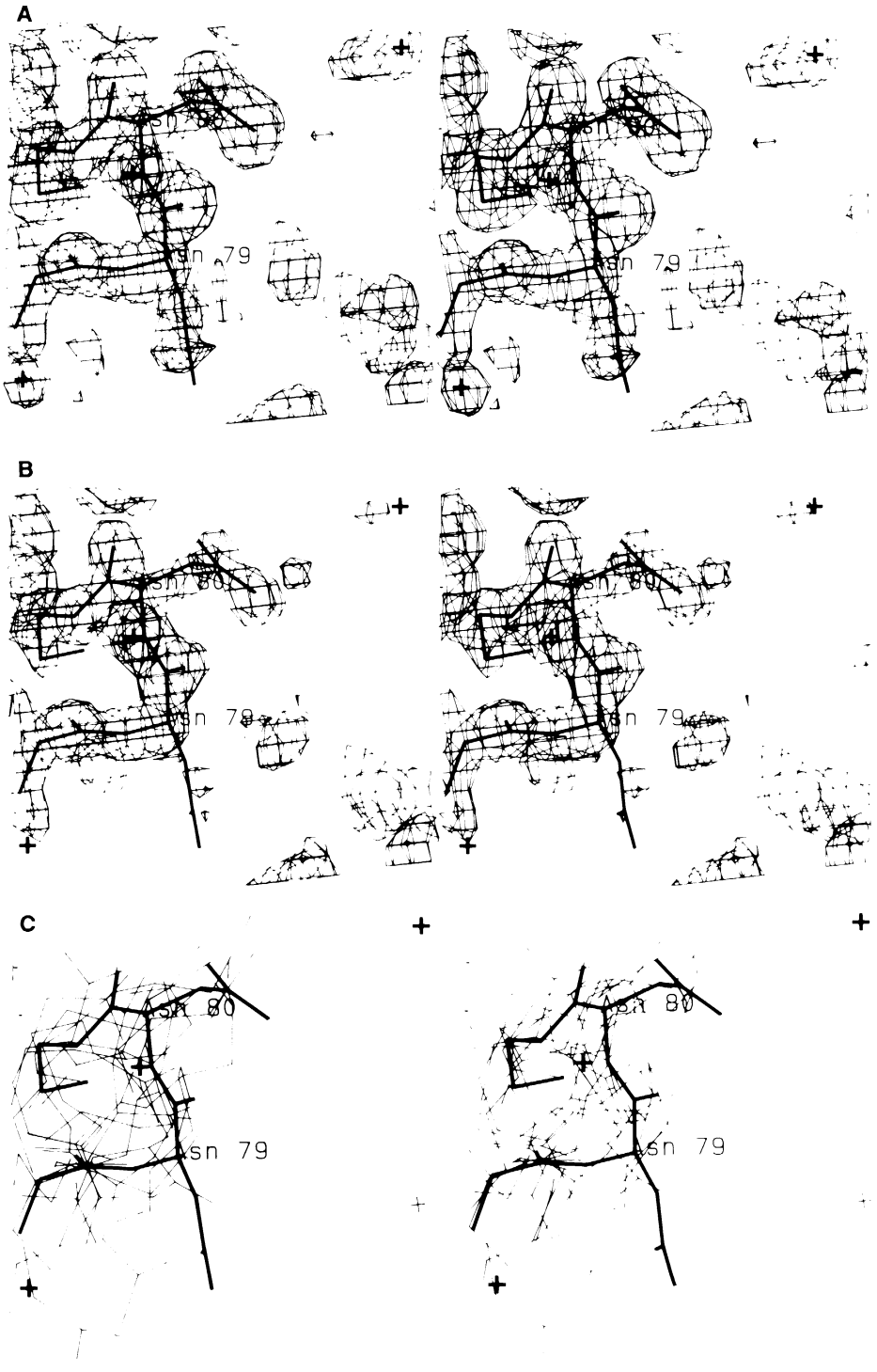

Fig. 3. Comparison of electron density around residues Asn^{79} and Asn^{80} based on the classical $\mathbf{F}_c$ (*10*) and on $\langle \mathbf{F}_c \rangle$ from $t = 40$ to 80 ps. (**A**) Electron density calculated with coefficients $(2|\mathbf{F}_o| - |\mathbf{F}_c|)\exp(i\alpha_c)$ contoured at 1σ. The thick lines show the atoms of the classically refined single site isotropic model (*10*) (see below). (**B**) Electron density calculated with coefficients $(2|\mathbf{F}_o| - |\langle \mathbf{F}_c \rangle|)\exp(i\alpha_{av})$ contoured at 1σ, where α_{av} stands for the phase of the average structure factor. The position of the classically refined model corresponds well with the electron density obtained by the procedure described in this report, although the atomic positions in individual structures of the ensemble vary considerably (see below). (**C**) Eight structures of $BPLA_2$ (thin lines) at 4-ps intervals from $t = 40$ ps onward.

lation it remains to be seen what the effects will be when the starting model contains large intrinsic errors. Moreover, for structures successfully refined at high resolution by classical procedures, the occurrence of large errors is most unlikely, and these structures are therefore good starting points to study the anisotropy and anharmonicity of the atomic distributions in the molecule by the method we present.

Time-averaged crystallographically restrained MD shows that phospholipase A_2 is more flexible than single site isotropic models obtained by classical crystallographic refinement techniques would suggest. Large deviations from the main conformation are observed, and these are likely to be important for the functioning of the molecule. Time-averaged crystallographically restrained MD, when applied to structure refinement, allows for more mobility and better searching of the conformational space, in comparison to least-squares methods and MD refinement procedures (*5, 6*), and provides a more complete representation of a biomacromolecule by calculating the ensemble of structures based on the experimental data. Accurate knowledge of molecular dynamics may prove useful in various fields of biochemistry.

REFERENCES AND NOTES

1. B. Howlin, D. S. Moss, G. W. Harris, *Acta Crystallogr. A* **45**, 851 (1989).
2. J. Kuriyan, G. A. Petsko, R. M. Levy, M. Karplus, *J. Mol. Biol.* **190**, 227 (1986).
3. W. F. van Gunsteren, H. J. C. Berendsen, J. Hermans, W. G. J. Hol, J. P. M. Postma, *Proc. Natl. Acad. Sci. U.S.A.* **80**, 4315 (1983).
4. W. F. van Gunsteren and H. J. C. Berendsen, GROningen MOlecular Simulation (GROMOS) library manual, BIOMOS Biomolecular Software (Laboratory of Physical Chemistry, University of Groningen, Groningen, 1987).
5. A. T. Brünger, J. Kuriyan, M. Karplus, *Science* **235**, 458 (1987).
6. M. Fujinaga, P. Gros, W. F. van Gunsteren, *J. Appl. Crystallogr.* **22**, 1 (1989).
7. A. E. Torda, R. M. Scheek, W. F. van Gunsteren, *Chem. Phys. Lett.* **157**, 289 (1989).
8. ———, *J. Mol. Biol.*, in press.
9. W. A. Pieterson, J. C. Vidal, J. J. Volwerk, G. H. de Haas, *Biochemistry* **13**, 1455 (1974).
10. B. W. Dijkstra, K. H. Kalk, W. G. J. Hol, J. Drenth, *J. Mol. Biol.* **147**, 97 (1981).
11. B. W. Dijkstra, J. Drenth, K. H. Kalk, *Nature* **289**, 604 (1981).
12. E. A. Dennis, *The Enzymes*, P. D. Boyer, Ed. (Academic Press, New York, 1983), vol. 16, pp. 307–353.
13. R. Renetseder, S. Brunie, B. W. Dijkstra, J. Drenth, P. B. Sigler, *J. Biol. Chem.* **260**, 11627 (1985).
14. The GROMOS (*4*)–MDXREF (*6*) program was adjusted according to Eqs. 1 and 2. For this purpose Eq. 2 was rewritten as: $\langle \mathbf{F}_c(\mathbf{s}) \rangle_{t'} = \exp\{-\Delta t/\tau_x\}\langle \mathbf{F}_c \rangle_{t'-\Delta t} + (1 - \exp\{-\Delta t/\tau_x\})\mathbf{F}_c^{t'}$ (where Δt is the time step in the simulation). This equation is equivalent to Eq. 2 when $t' >> \tau_x$. The simulation was performed in vacuo with all protein atoms and 106 crystal water molecules of $BPLA_2$. The GROMOS 37D4 force field of (*4*) was used with the SHAKE algorithm to constrain the bond lengths (*15*) and with time steps of 2 fs. From $t = 0$ ps to 16 ps the individual isotropic temperature factors of each atom were gradually reduced to 1 $Å^2$ for all atoms, while τ_x was increased from 0 to 4 ps. At $t = 20$ ps τ_x was increased to 8 ps and at $t = 26$ ps to $\tau_x = 16$ ps. Up to $t = 28$ ps the temperature was coupled to a bath (*16*) of 150 K with a temperature-relaxation time, τ_T, of 0.012 ps; afterward the bath temperature was set to 200 K. During the whole run σ_x was kept at 140 (arbitrary units), which is roughly equivalent to $(\langle(|\mathbf{F}_o| - |\mathbf{F}_c|)^2\rangle)^{1/2})$ at $t = 0$ ps. All of the x-ray data between 8.0 and 1.7 Å resolution with $|\mathbf{F}_o| > \sigma_{\mathbf{F}o}$ were used in the calculations. Heating was observed in the presented simulation. The amount of heating depends on the magnitude of τ_x; for $\tau_x = 4$ ps, $\Delta T = 108$ K, for $\tau_x = 8$ ps, $\Delta T = 56$ K, and for $\tau_x = 16$ ps, $\Delta T = 30$ K, where ΔT is defined as $\langle T \rangle - T_{bath}$. The average potential energy of the simulated system observed from $t = 40$ to 80 ps is -4.52×10^3 kJ/mole, compared with -5.31×10^3 kJ/mole for an unrestrained simulation of $BPLA_2$ in vacuo at 300 K. A related measure is the average root-mean-square deviations from standard geometry of the structures from the ensemble, which are 0.015 Å for bond lengths, 4.2° for bond angles, and 28° for torsion angles, as calculated by the program TNT (*17*) from a subset of structures taken at 4-ps intervals from the ensemble.
15. J. P. Ryckaert, G. Ciccotti, H. J. C. Berendsen, *J. Comput. Phys.* **23**, 327 (1977).
16. H. J. C. Berendsen, J. P. M. Postma, W. F. van Gunsteren, A. Dinola, J. R. Haak, *J. Chem. Phys.* **81**, 3684 (1984).
17. D. E. Tronrud, L. ten Eyck, B. W. Matthews, *Acta Crystallogr. A* **43**, 489 (1987).
18. O. P. Kuipers *et al.*, *Science* **244**, 82 (1989).
19. M. P. Allen and D. J. Tildesley, *Computer Simulation of Liquids* (Clarendon, Oxford, 1987).
20. J. Hermans, H. J. C. Berendsen, W. F. van Gunsteren, J. P. M. Postma, *Biopolymers* **23**, 1513 (1984).
21. A. T. Brünger, *J. Mol. Biol.* **203**, 803 (1988).
22. M. G. Vincent and J. P. Priestle, *J. Appl. Crystallogr.* **18**, 185 (1985).

23. We thank A. E. Torda and M. Fujinaga for helpful and stimulating discussions and B. W. Dijkstra for generously supplying the x-ray diffraction data of phospholipase. Supported by the Dutch Foundation for Chemical Research (SON) with financial aid from the Dutch Organization for Scientific Research (NWO).

24 April 1990; accepted 25 July 1990

Possible Early Pennsylvanian Ancestor of the Cycadales

RICHARD L. LEARY

A specimen of *Lesleya*, previously known only as isolated sterile foliage, has been found with two rows of ovule-bearing receptacles on opposite sides of the petiole. This specimen is from the Lower Pennsylvanian (Namurian B or C) of western Illinois. The fertile portion of this specimen is similar to *Phasmatocycas kansana* Mamay from the Lower Permian of Kansas and Texas, which Mamay interpreted as an ancestral form to cycads. *Phasmatocycas* was found attached to the base of *Taeniopteris* by Gillespie and Pfefferkorn. The foliar portions, *Lesleya* and *Taeniopteris*, have many features in common; the major morphologic difference is curvature of the veins. *Lesleya* and its attached fertile petiole are proposed as ancestors of *Taeniopteris* and *Phasmatocycas*, and ultimately, the ancestors of modern cycads. This extends the age of known precursors of cycads back from the Early Permian to Early Pennsylvanian (about 320 million years ago), approximately 35 million years earlier.

DURING THE PAST 20 YEARS, several fossil discoveries have shed light on the question of the origin of cycads. Delevoryas (*1*) suggested an origin within the medullosan pteridosperms. He suggested that cycads and cycadeoids were derived from slender plants bearing compound leaves. He (*2*) compared the Pennsylvanian pinnately compound *Eremopteris zamioides* (Bertrand) Kidston and Permian *Tinsleya texana* Mamay to compound early cycad foliage.

Mamay (*3*), on the other hand, in describing *Archaeocycas* and *Phasmatocycas*, suggested that cycads were derived from plants with entire leaves. This was borne out by Gillespie and Pfefferkorn (*4*) who found *Taeniopteris* attached to *Phasmatocycas*. The material described here provides additional evidence that cycads were derived from plants with entire leaves and that compound leaves were derived as suggested by Mamay [figure 11 of (*5*)].

Department of Geology, Illinois State Museum, Springfield, IL 61706.

Several sites in western Illinois have yielded significant information about Early Pennsylvanian nonswamp floras, both on their overall composition and on individual taxa within the floras (*6, 7*). The Allied Stone Company quarry in Milan, Illinois, (*8*) has been a major collecting site for nearly 15 years and continues to produce new species and genera as well as new data on known taxa.

Specimens described here were collected from Lower Pennsylvanian sedimentary rocks which fill channels eroded in the Devonian Cedar Valley Limestone (*8*). The fossil-bearing strata consist of shale, siltstone, sandstone, and occasional thin conglomerate.